centers are aggregated into clusters of local high density, then spin-diffusion suppression is expected to be much more severe; this situation can be described within the framework of our approach to the spin-diffusion equations and will be the subject of a subsequent publication.

*Work supported by the U. S. Air Force Office of Scientific Research under Grant No. AFOSR-69-1749.

†Present address: Physics Department, University of Illinois, Urbana, Ill.

[1]C. P. Slichter and D. C. Ailion, Phys. Rev. 135, A1099 (1964).

[2]D. C. Ailion and C. P. Slichter, Phys. Rev. 137, A235 (1965).

[3]M. Kumano and M. Hanabusa, J. Phys. Soc. Japan 25, 1282 (1968).

[4]Jerome Wagner, thesis, University of Wisconsin, 1969 (unpublished).

[5]J. Wagner and P. R. Moran (unpublished), referred to as WM in the text.

[6]S. R. Hartmann and E. L. Hahn, Phys. Rev. 128, 2042 (1962).

[7]A. G. Redfield, Phys. Rev. 130, 589 (1963).

[8]F. M. Lurie and C. P. Slichter, Phys. Rev. 133, A1108 (1964).

[9]R. E. Walstedt, D. A. McArthur, and E. L. Hahn, Phys. Letters 15, 7 (1965).

[10]A. Hartland, Proc. Roy. Soc. (London) A304, 361 (1968).

[11]G. T. Mallick and R. T. Schumacher, Phys. Rev. 166, 350 (1968).

[12]K. F. Nelson and W. D. Ohlsen, Phys. Rev. 180, 366 (1969).

[13]Y. Tsutsumi, M. Kunitomo, and T. Hashi, J. Phys. Soc. Japan 20, 2095 (1965).

[14]D. V. Lang and P. R. Moran, Phys. Rev. B 1, 53 (1970), referred to as LM in the text.

[15]D. V. Lang, thesis, University of Wisconsin, 1969 (unpublished).

[16]P. R. Spencer, thesis, University of Illinois, 1969 (unpublished).

[17]P. R. Spencer, H. D. Schmid, and C. P. Slichter, Phys. Rev. B 1, 2989 (1970).

[18]N. Bloembergen, Physica 15, 386 (1949).

[19]P. G. de Gennes, J. Phys. Chem. Solids 7, 345 (1958).

[20]W. E. Blumberg, Phys. Rev. 119, 79 (1960).

[21]G. R. Khutsisvili, Usp. Fiz. Nauk 87, 211 (1965) [Soviet Phys. Usp. 8, 743 (1966)].

[22]I. J. Lowe and D. Tse, Phys. Rev. 166, 279 (1968).

[23]R. E. Slusher and E. L. Hahn, Phys. Rev. 166, 332 (1968), referred to as SH in the text.

[24]A. G. Redfield and W. N. Yu, Phys. Rev. 169, 443 (1968).

[25]D. A. McArthur, E. L. Hahn, and R. E. Walstedt, Phys. Rev. 188, 609 (1969).

PHYSICAL REVIEW B VOLUME 2, NUMBER 7 1 OCTOBER 1970

Electron-Impact Desorption of Ions from Polycrystalline Tungsten*

Mitsuaki Nishijima†
Coordinated Science Laboratory and Department of Electrical Engineering, University of Illinois, Urbana, Illinois 61801

and

Franklin M. Propst
Coordinated Science Laboratory and Department of Physics, University of Illinois, Urbana, Illinois 61801

(Received 21 January 1970)

A cylindrical magnetic spectrometer has been constructed to study the electron-impact desorption of ions and neutrals from solid surfaces. The instrument has high-energy resolution and sensitivity and allows the determination of the charge-to-mass ratio of the emitted ions. The apparatus has been applied to the study of polycrystalline tungsten with O_2, CO, CO_2, H_2, N_2, and H_2O adsorbed. The ions which have been observed are O^+ from O_2/W, CO/W, and CO_2/W; CO^+ from CO/W; and H^+ from H_2/W and H_2O/W. The ion energy distributions, ionic and total desorption cross sections, threshold energies, and other experimental results are presented and discussed.

I. INTRODUCTION

The process of the emission of ions by electron bombardment was first reported by Dempster in 1918.[1] However, before 1964, little was known about the mechanism involved in the electron-impact desorption of ions and neutrals from solid surfaces. In 1964, Redhead[2] and Menzel and

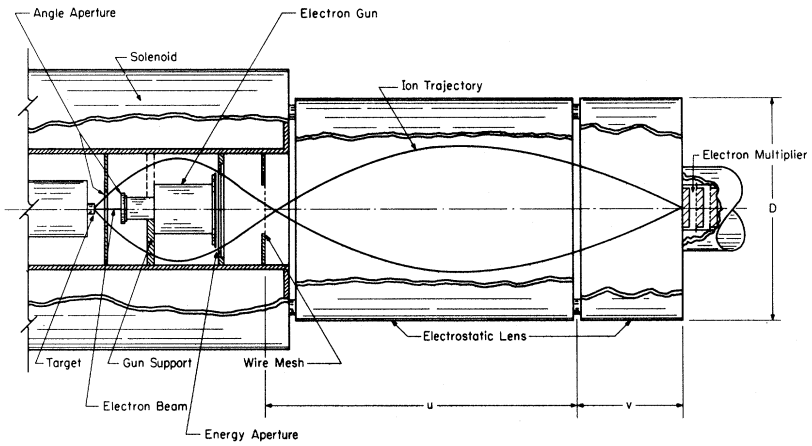

FIG. 1. Schematic of cylindrical magnetic spectrometer. A schematic ion trajectory is also shown.

Gomer[3] independently proposed a mechanism for the process and used it in the study of solid surfaces, opening a promising field of research. The model which has been proposed is similar to that by which energetic ions are produced by the electron bombardment of molecules in the gas phase. In this model, an atom in the ground state is excited to an ionic state by an incident electron. If the interaction potential for the ionic state is repulsive, energetic ions are evolved. The main difference between a molecule in the gas phase and an atom adsorbed on a metallic surface is that in the latter case there is a high probability that the ion will be neutralized through an Auger process before separation can occur. Thus, the cross sections for ionic desorption are typically much smaller than the cross sections for excitation to metastable or ionic states in gases. A more detailed description of the model will be given in a later section in conjunction with a calculation of the energy distributions of emitted ions.

Electron-impact desorption has been studied using ionization gauges,[4–8] mass spectrometers,[5–19] field-emission microscopes,[3,20–22] and retarding field analyzers.[2,6,23–26] These instruments have provided much valuable information; however, a review of the literature indicates the need for an instrument with higher energy resolution and greater sensitivity. In addition, it would be advantageous to measure in one apparatus energy distributions and the charge-to-mass ratios of the ions. We have designed and constructed a cylindrical magnetic spectrometer (Fig. 1) which accomplishes each of these objectives.

The instrument has been applied to the study of polycrystalline tungsten with O_2, CO, H_2, N_2, CO_2, and H_2O adsorbed. The quantities which have been measured are: ion species desorbed, ion energy distributions, ionic and total (ion plus neutral) desorption cross sections, and threshold energies. These results are presented in the following sections. We have also made measurements of the kinetics of the adsorption-desorption processes and some measurements of thermal processes. The details of these measurements will be reported elsewhere.[27]

II. APPARATUS AND PROCEDURE

The instrument which has been designed for this work is essentially a small β-ray spectrometer of the axially symmetric type. The spectrometer, which is housed in an ultrahigh-vacuum system, incorporates an electron gun, a target, an angle aperture, an energy aperture, baffling apertures, an electrostatic lens system, and a collector (electron multiplier). The electron gun, which is placed on the axis of the apparatus, produces an electron beam which impinges on the target (also located on the axis). The ions produced by this bombardment follow helical trajectories in the axial magnetic field applied by the solenoid. Only those ions in a particular range of angle and energy pass through the apertures. Ions are analyzed by varying the magnetic field or the bias voltage between the target and the aperture system. The ions are focused onto an electron multiplier by an electrostatic lens system.

The characteristics of the instrument are: (a) ~4% energy resolution, (b) sufficient sensitivity to allow energy distribution measurements of systems with ion yields (number of ions desorbed per electron) as low as 10^{-9} ions per electron, and (c) a mass resolution of ~8% (for the ion energies and energy spreads typical for electron-impact ionization). Tests indicate that the electron gun can deliver a current of up to 10^{-4} A with a beam spot size of ~1 mm diam, over an energy range from zero to 600 eV. The 16-stage, BeCuO venetian-

blind electron multiplier has a gain of $\sim 10^5$. The stainless-steel bakeable ultrahigh-vacuum system used for the present work includes a 400-liter/sec sputter ion pump, and a titanium sublimation pump. It has been found that a total pressure of $\sim 5\times10^{-10}$ Torr can be achieved in about one and one-half days from the start of the pumpdown. The pressure subsequently drops to $\sim 1\times10^{-10}$ Torr in a few more days. The details of the design and construction of the apparatus will be reported elsewhere.[28]

The tungsten sample (8.25 mm diam) was cut from a sheet of 0.13-mm-thick polycrystalline tungsten obtained from the Kulite Corp. An analysis supplied with the material shows a tungsten purity of 99.95% with carbon present at 30 ppm, and hydrogen at 6 ppm. After machining, the target was electropolished to about 0.1 mm thickness to remove surface contamination. The target was then installed in the apparatus, and the steps followed in cleaning were:

(1) Heat the target for an hour or more in vacuum to over 2200 °K (electron bombard the target at 0.2 A and 1000 V). Heat until the pressure bursts, due to flashing the target to over 2200 °K, are less than 1×10^{-9} Torr.

(2) Heat the target for about 24 h to over 2200 °K in about 1×10^{-6} Torr of oxygen to remove surface contamination due to the outward diffusion of interstitial carbon.[29]

(3) Flash the target to over 2200 °K for about 3 sec two to three times before each measurement.

As a rough check of surface cleanliness, the instrument is used to verify that no surface ions are produced after flashing. Reproducibility of the experimental data is always examined as an additional check of the surface cleanliness.

In this work we could not accurately determine the temperature of our target. The target temperature for the measurements presented here is probably slightly higher than 300 °K.

The methods used for the measurement of the ion species, ion energy distributions, ion yield, total desorption cross sections, and the time-dependent measurements are described elsewhere.[27]

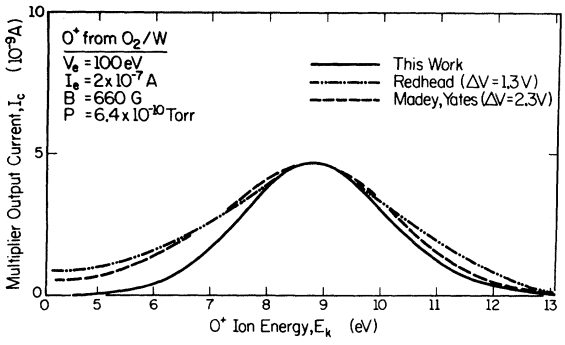

FIG. 2. Energy distribution of O^+ ions from tungsten fully covered with O_2. The energy scale is corrected for the contact potential between the target and the analyzer. For comparison, the data of Redhead (Ref. 24) and Madey and Yates (Ref. 26) are included. The distributions are normalized, and plotted such that the maxima are at the same energy. The energy shift necessary to accomplish this is indicated by ΔV.

III. EXPERIMENTAL RESULTS

The states of adsorption and the electron-impact desorption parameters for the various systems are summarized in Table I. The experimental curves are shown in Figs. 2–10. In the figures, V_e is electron energy, I_e is electron current, V_B is target bias, E_k is ion kinetic energy, and I_c is electron-multiplier output current.

A. Ion Species

We have observed O^+ ions from O_2/W, CO/W, and CO_2/W, CO^+ ions from CO/W, and H^+ ions from H_2/W and H_2O/W. No other ions were observed in any of the systems. The N_2/W system was also studied, but no ions were observed.

B. Ion Energy Distributions

Except for the H_2/W system, the energy distributions of ions have been measured at an incident electron energy V_e of 100 eV, and an electron current I_e of 2×10^{-7} A. It is found that this value of electron current is sufficiently small that the electronic desorption is negligible during a sweep of the ion energy distribution.

Figure 2 shows the energy distribution of O^+ ions from tungsten fully covered with oxygen. The distribution has a maximum at 8.8 eV and a half-width of 3 eV. The ion energy extends from approximately 5–13 eV, and the distribution is symmetrical about the maximum. The energy scale is corrected by 1.7 eV for the contact potential between the target and the analyzer. This correction is accurate to $\sim\pm0.5$ eV and is determined by studying the elastic reflection of electrons from the target. The contact potential between the target and the cathode is determined by the retarding-potential technique.

For comparison, the results of Redhead[24] and Madey and Yates[26] are also shown in Fig. 2. The distributions are normalized and are plotted such that the maxima are at the same energy. Redhead found the maximum at 7.5 eV with an indicated error in the energy scale of ±0.5 eV. Madey and Yates found the peak at 7.5 eV. They report a correction of 1 eV for the work-function difference between the oxygen-covered tungsten target and the oxygen-covered Cu collector, leading to the cor-

TABLE I. Summary of ion-energy distribution and electron-impact desorption parameters obtained in this work. (V_e = 100 eV, except for H_2/W where V_e = 300 eV.)

Adsorbed gas	O_2/W		CO/W			H_2/W	N_2/W	CO_2/W		H_2O/W
State	State 1	State 2	State 1	State 2	State 3	State 1	•••	State 1	State 2	State 1
Ion	•••	O^+	CO^+	O^+	CO^+	•••	H^+	•••	•••	O^+	H^+
Ion energy at "peak" (eV)[a]	•••	8.8	1.3	7.9	(1.3)	•••	1.7	•••	•••	5.7	4.1
Half-width of ion energy distribution (eV)	•••	3	1.6	2.8	(1.6)	•••	1.7	•••	•••	2.5	4.8
Ion yield (ions/electron)	$<10^{-9}$	8×10^{-6}	8×10^{-7}	3×10^{-6}	$\sim 8\times10^{-8}$	$<10^{-9}$	6×10^{-9}	$<10^{-9}$	$<10^{-9}$	2×10^{-7}	6×10^{-7}
Ion desorption cross section (cm^2)	$< 2\times10^{-24}$	3×10^{-19}	5×10^{-21}	1.5×10^{-20}	$\sim 4\times10^{-22}$	$< 5\times10^{-24}$	3×10^{-23}	$<5\times10^{-24}$	$<5\times10^{-24}$	1×10^{-21}	3×10^{-21}
Total desorption probability (neutrals or ions/electron)	•••	9×10^{-5}	•••	5×10^{-4}	5×10^{-4}	•••	•••	•••	•••	4×10^{-4}	•••
Total desorption cross section (cm^2)	•••	3×10^{-18}	•••	$2-3\times10^{-18}$	$2-3\times10^{-18}$	•••	•••	•••	•••	2×10^{-18}	•••
Ratio of neutrals to ions	•••	10	•••	150	6000	•••	•••	•••	•••	2000	•••
Assumed surface coverage (particles/cm^2)[b]	5×10^{14}	3×10^{13}	1.5×10^{14}	2×10^{14}	2×10^{14}	2×10^{14}	2×10^{14}	2×10^{14}	2×10^{14}	2×10^{14}	2×10^{14}
Threshold energy for ion desorption at "peak" (eV)[a]	•••	20.5	15.5	18.5	•••	•••	•••	•••	•••	•••	•••

[a] "Peak" is the maximum in the energy distribution of ions.

[b] The surface coverage is used to obtain the ion-desorption cross section from the ionization probability, and the total desorption probability from the total desorption cross section. The values used are reported by other workers.

rected maximum at 6.5 eV. Since oxygen-covered copper has a work function of ~5 eV and oxygen-covered tungsten ~6 eV,[30,31] it would appear that their correction was in the wrong direction and should have been to 8.5 eV.

Our data agree quite well with those of other workers in the higher-energy region, but large differences exist in the low-energy region. The differences can easily result from the electron optics of the retarding-field analyzers used by these workers. The comparatively low ion energy they observed for the maximum might be due to the same effect.[28]

Figure 3 shows the O^+ ion energy distribution from tungsten fully covered with oxygen as a function of electron energy V_e. For $V_e \lesssim 30$ eV, the ion energy distributions shift to lower energies. This is predicted by the model mentioned above. For $V_e \gtrsim 30$ eV, the distributions have maxima at ~8.8 eV, and show little change in shape with V_e.

The O^+ ion energy distributions have been measured as a function of coverage during oxygen adsorption and during desorption by electron bombardment. For these latter measurements, the desorption rate was increased by increasing the incident electron current by a factor of 10–100. The O^+ ion energy distributions for different coverages are nearly identical in shape, indicating that the state which produces O^+ ions (state 2) is a single state in the coverage range studied.

The ion current from state 1 (the state populated at low coverage[27]) was at least a factor of 10^4 smaller than from state 2, and was too small to allow measurements of the ion energy distribution.

Figure 4 shows the O^+ ion energy distribution from tungsten fully covered with CO. A 0.9-eV correction was made to the energy scale for the contact potential between the CO-covered target and the analyzer. This correction was chosen such that the CO^+ ion (which is also observed) has a minimum energy of at 0 eV. (Fig. 5). The ion energy scale may be in error by ±0.5 eV. The O^+ ion distribution has a maximum at 7.9 eV, is quite symmetrical about this maximum, has a half-width of 2.8 eV, and extends from ~4–12 eV.

The results of Redhead[24] and Coburn[18] are also shown in Fig. 4. These curves are normalized to our data at the O^+ ion peak. Their data agree well with ours at the high-energy region, but there are substantial differences in the low-energy region. Again, this is attributed to the electron optics of the analyzers used.

Figure 5 shows the CO^+ ion energy distribution for tungsten fully covered with CO. Because of

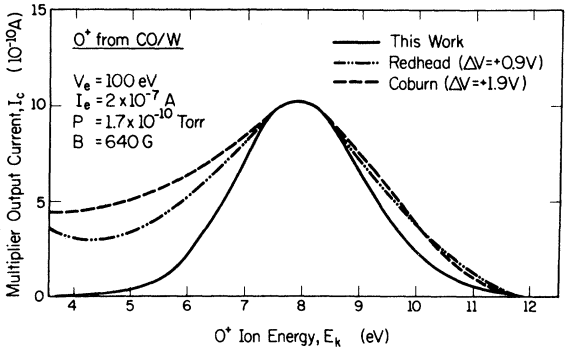

FIG. 4. Energy distributions of O^+ ions from tungsten fully covered with CO. The energy scale is set so that the lower edge of the distribution of CO^+ ions is at zero eV. For comparison, the data of Redhead (Ref. 24) and Coburn (Ref. 18) are included. The distributions are normalized and plotted such that the maxima are at the same energy. The energy shift necessary to accomplish this is indicated by ΔV.

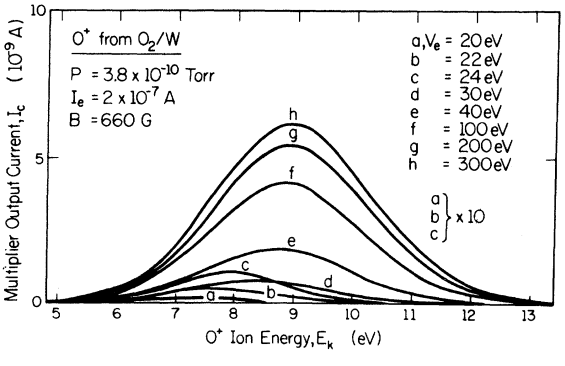

FIG. 3. Energy distributions of O^+ ions from O_2/W for various incident electron energies. The electron energy is not corrected for the contact potential between the target and the cathode of the electron gun.

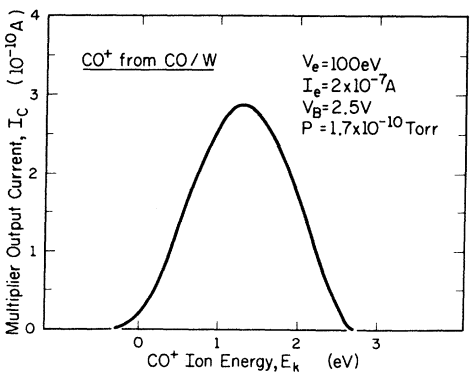

FIG. 5. Energy distribution of CO^+ ions from tungsten fully covered with CO. The energy scale is set so that the lower edge of the distribution is at 0 eV.

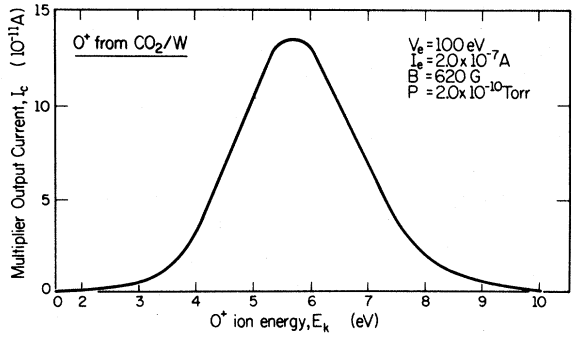

FIG. 6. Energy distribution of O^+ ions from tungsten fully covered with CO_2. The energy scale is not corrected for the contact potential between the target and the analyzer.

the combination of mass and ion energy, the high-energy region of the CO^+ ion distribution overlaps the low-energy region of the O^+ ion distribution. We have obtained the CO^+ ion energy distribution by subtracting the O^+ ion energy distribution. The maximum of the CO^+ ion energy distribution is at 1.3 eV (with the contact potential correction described above), the half-width is 1.6 eV, and it extends from 0 to ~3 eV. The shapes of the O^+ and CO^+ ion energy distributions were almost independent of the coverage.

Figure 6 shows the energy distribution of O^+ ions from tungsten fully covered with CO_2. The distribution has a maximum at 5.7 eV, is symmetrical about the maximum, and has a half-width of 2.5 eV. The energy scale is not corrected for the contact potential between the target and the analyzer.

The energy distributions of H^+ ions from tungsten fully covered with H_2, and H_2O are shown in Fig. 7. In both cases the energy scale is fixed such that the low-energy edge of the distribution is at zero energy. Both distributions are quite asymmetrical and have long tails towards higher energies; however, the distribution for H_2/W has a maximum at ~1.7 eV, a half-width of 1.7 eV, and extends from ~0 to 6 eV, while the distribution from H_2O/W has a maximum at ~4.1 eV, a half-width of 4.8 eV, and extends from ~0 to 14 eV. Another striking difference between the two systems is that the ion yield for the H_2O/W system is ~100 times greater than for H_2/W system. Because of the low yield for H_2/W, the energy distribution measurement was made at $I_e = 2\times10^{-6}$ A and $V_e = 300$ eV.

C. Ion Desorption Cross Sections

Figure 8 shows the ion current for 8.8-eV O^+ from tungsten fully covered with oxygen as a function of V_e. For $V_e \lesssim 100$ eV, the O^+ ion current increases sharply with V_e, and for $V_e \gtrsim 100$ eV it increases very slowly. Because of a slight variation in the size of the electron beam at the target as V_e is varied, our measurement shows some structure in this type of curve. The amplitude of this structure is indicated by error bars. By making several measurements at different values of magnetic field, this structure averages out, and the solid curve (which is the average of several measurements) is felt to be more accurate than indicated by the error bars. Figure 8 also shows the ion currents for 7.9-eV O^+ from CO/W, 1.3-eV CO^+ from CO/W, 5.7-eV O^+ from CO_2/W, 1.7-eV H^+ from H_2/W, and 4.1-eV H^+ from H_2O/W as a function of electron energy. These energies correspond to the maxima in the various ion energy distributions. The dependence of the O^+ ion current on electron energy in the other systems is quite similar to that observed for the O^+ ion current from O_2/W. We had some difficulty in the measurement of H^+ ion current from H_2-covered tungsten because of the low H^+ ion current. The curve shows a significant increase in the ion current as a function of V_e beyond $V_e = 100$ eV. This behavior is quite different from the dependence of the H^+ ion current from water-vapor-covered tungsten.

Figure 9 shows a comparison of the variation of the ion desorption cross section and total desorption cross section for oxygen-covered tungsten with electron energy. The two quantities are normalized at $V_e \simeq 150$ eV. The total desorption cross sections for various electron energies are determined from the time dependence of electron desorption measurements.[27] It will be noted that for $V_e \gtrsim 40$ eV, the two cross sections show a very similar dependence on electron energy, while for $V_e \lesssim 40$ eV the curves are different, and the total desorption cross section exhibits a different threshold than that for ion desorption. It should be em-

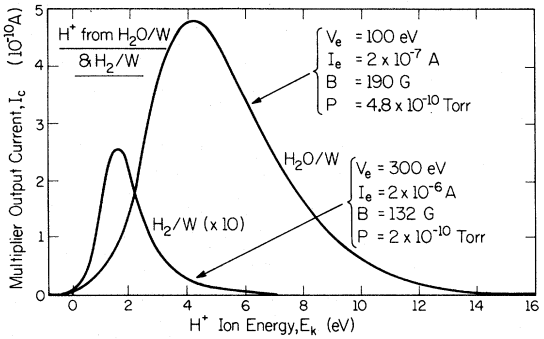

FIG. 7. Energy distributions of H^+ ions from tungsten covered with H_2 and H_2O. The energy scale is set so that the lower edge of the distribution is at 0 eV.

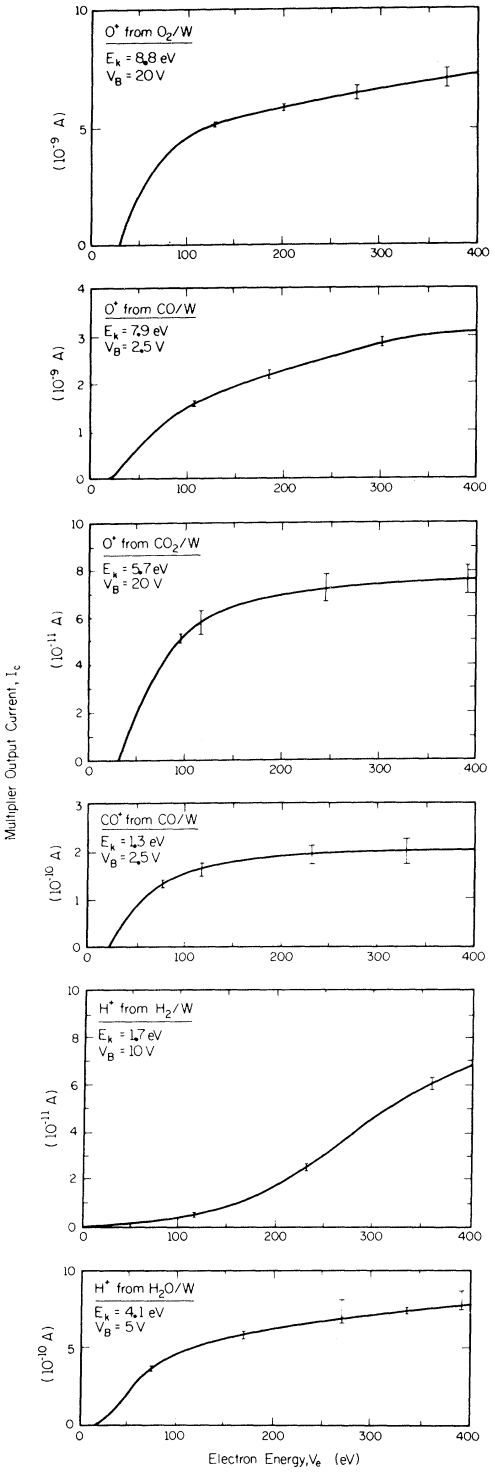

FIG. 8. Dependence of the O^+ ion current from O_2/W, CO/W, and CO_2/W; the CO^+ ion current from CO/W; and the H^+ ion current from H_2/W; and H_2O/W on the electron energy. The energy scale is not corrected for the contact potential between the target and the cathode of the electron gun.

phasized that the measurement of the total desorption cross section at very low electron energies is difficult and is not extremely accurate; however, the accuracy is sufficient to give strong indication of two mechanisms in the total desorption cross section. The first mechanism appears to have a threshold at a few eV below the ion production threshold. Thus, this mechanism for neutral desorption is not the neutralization of ions, but probably corresponds to excitation directly to antibonding neutral states. However, since the curve for the total desorption cross section breaks at an energy close to the threshold energy for ion production and at higher energies follows closely the curve for the ion desorption cross section, it would appear that the neutralization of ions is in fact a dominant mechanism for neutral desorption. In his study of the CO/W system, Menzel[19] found that the variation of the CO^+ ion desorption cross section with electron energy was quite different from the variation of the total desorption cross section. It is likely that the reason for this large difference is the experimental error involved in determining ion desorption cross sections with his apparatus.[28]

In the apparatus used in this work it is difficult to determine absolute ion yields accurately since this requires the knowledge of the angular distribution of desorbed ions as well as the determination of the transmission of the spectrometer and the current gain of the electron multiplier. To estimate ion yields, we have assumed that the angular distribution of the emitted ion is a cosine distribution, that the transmission efficiency of the analyzer is unity, and that the total current gain of the multiplier is $\sim 10^5$. The ion desorption cross sections are calculated from the estimates of ion yields using the surface coverage estimated by

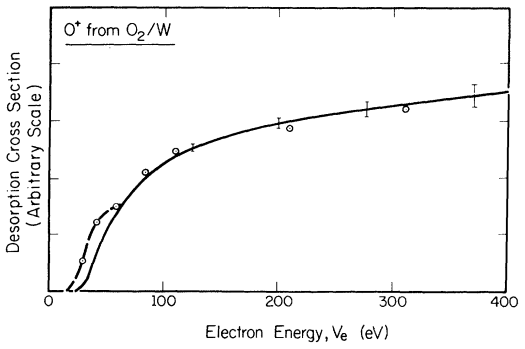

FIG. 9. Comparison of the variation with electron energy of the total desorption cross section (open circles) and the ion desorption cross section (solid curve) for O_2/W. The two quantities are normalized at $V_e \simeq 150$ eV. The error bars pertain to the ion desorption cross section.

other workers. A summary of the desorption parameters (some of which are based on these assumptions) is given in Table I.

D. Threshold Energies

Figure 10 shows the data used for the determination of the threshold energy for the liberation of O^+ ions from oxygen-covered tungsten. The threshold for O^+ ions with 8.8-eV energy (corresponding to the maximum in the energy distribution) is 20.5 eV. The thresholds for ions with energies corresponding to the half-height points of the energy distribution (7.3 and 10.3 eV) are 19.0 and 22.0 eV. Thus, there is a linear dependence of threshold energy with ion energy as is expected from the theoretical model. It is difficult to measure accurately the threshold energy because the ion current increases almost exponentially with electron energy near the threshold. The average of several experiments is used to determine the threshold energy. The threshold energy did not vary with coverage within our experimental error. The experimental value of the threshold energy has been corrected for the work-function difference between the cathode and the oxygen-covered tungsten target.

In making threshold measurements with retarding-potential analyzers, the retarding potential is generally set at zero so that ions with all energies above zero are collected. The threshold determined in this way is then the threshold for the production of ions with energy equal to the low-energy cutoff of the ion energy distribution. In addition, since ions at all emission energies are detected and since there is a different threshold for each ion energy, such measurements can be difficult to interpret. Similar remarks hold for measurements made with mass spectrometers. However, if done properly, these measurements should lead to the threshold for production of ions with an energy equal to the low-energy cutoff. We shall designate this threshold as the "minimum threshold."

Madey and Yates[26] measured the minimum threshold energy for the production of ions from O_2/W to be 19.3 eV. Since we find that the low-energy cutoff of the ion energy distribution is ~5 eV, their measurement would predict a threshold of 23.1 eV for 8.8-eV ions (as opposed to the value of 20.5 eV measured in this work).

The measurements of the threshold energies for the desorption of O^+ and CO^+ ions from tungsten covered with CO were made in a manner similar to those for the O_2/W system. The threshold energy for O^+ ions with 7.9-eV energy (corresponding to the maximum in the energy distribution) is found to be 18.5 eV, and again the threshold is found to increase approximately linearly with ion energy. The threshold energy for desorption of 1.3-eV CO^+ ions is 15.5 eV.

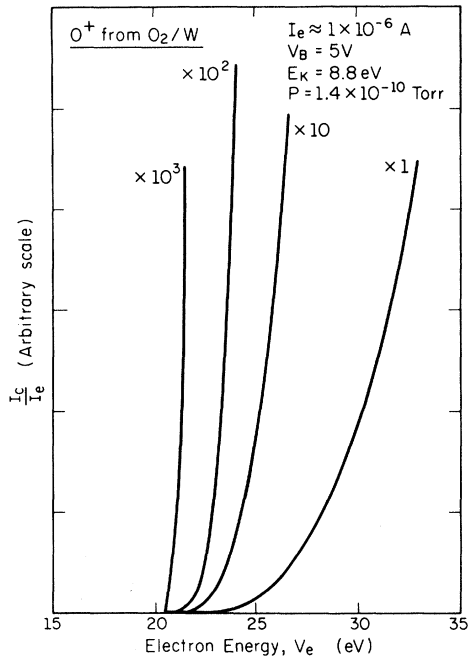

FIG. 10. Dependence of the O^+ ion current from O_2/W on the electron energy in the region of the threshold. The energy scale is corrected for the contact potential between the target and the cathode of the electron gun.

Table II shows the threshold energies which have been measured in this work along with those reported by other workers. The column labeled "Normalized threshold" gives the values for the emission of ions with energy equal to that of the maximum in the energy distribution. This normalization is made as indicated above. The discrepancies among the workers will be discussed later.

IV. DISCUSSION

A. Ion Energy Distribution

The theoretical model for the electron-impact desorption of ions was suggested by Redhead[2] and by Menzel and Gomer.[3] The experimental observations which the theory must explain are:

(1) Both ions and neutrals are desorbed.

(2) Desorption can occur from tightly bonded states.

(3) The desorbed particles can possess considerable kinetic energy (from 0 to $\gtrsim$10 eV).

(4) Desorption cross sections vary over a wide range (10^{-17} to $<10^{-21}$ cm^2) and are typically very small compared to ionization or excitation cross sections for gaseous atoms or molecules.

We shall apply a simple one-dimensional model to the calculation of the electron-impact desorption of O^+ ions from O_2/W and CO/W. The calcula-

TABLE II. Comparison of the threshold energy of ion desorption obtained by various workers.

System	Ion	Worker	"Minimuum threshold energy" (eV)[a]	Normalized threshold (eV)	Theoretical threshold energy (eV),[b] final states of the two electrons at Vacuum level	Fermi level
O_2/W	O^+	Yates *et al.* (Ref. 25)	21.8 ($E_k = \sim 5$)	~ 25.6 ($E_k = 8.8$)	28.9	17.1
		Madey, Yates (Ref. 26)	19.3 ($E_k = \sim 5$)	~ 23.1 ($E_k = 8.8$)	($E_k = 8.8$ eV)	($E_k = 8.8$)
		This work	20.5 ($E_k = \sim 8.8$)[c]	20.5 ($E_k = 8.8$)		
CO/W	O^+	Redhead (Ref. 24)	20.5 ($E_k = \sim 4$)	~ 24.4 ($E_k = 7.9$)	26.7	16.1
		Yates *et al.* (Ref. 25)	17.3 ($E_k = \sim 4$)	~ 21.2 ($E_k = 7.9$)	($E_k = 7.9$)	($E_k = 7.9$)
		Coburn (Ref. 18)	20.9 ($E_k = 4.7$)[c]	24.1 ($E_k = 7.9$)		
		Menzel (Ref. 19)	20.0 ($E_k = \sim 4$)	~ 23.9 ($E_k = 7.9$)		
		This work	18.5 ($E_k = 7.9$)[c]	18.5 ($E_k = 7.9$)		
CO/W	CO^+	Redhead (Ref. 24)	15.1 ($E_k = \sim 0$)	~ 16.4 ($E_k = 1.3$)	16.4	5.8
		Yates *et al.* (Ref. 25)	17.3 ($E_k = \sim 0$)	~ 18.6 ($E_k = 1.3$)	($E_k = 1.3$)	($E_k = 1.3$)
		Menzel (Ref. 19)	14.6 ($E_k = \sim 0$)	~ 15.9 ($E_k = 1.3$)		
		This work	15.5 ($E_k = 1.3$)[c]	15.5 ($E_k = 1.3$)		

[a]The "minimuum threshold energy" is defined in Sec. III D. The kinetic energy of the corresponding ions is an estimate based on the energy distributions measured in this work.

[b]Assumptions used in this calculation are given in the discussion of threshold energies.

[c]The threshold energy for these measurements is for ions of the kinetic energy specified.

tion is similar to that reported by Redhead[2]; however, we shall perform the numerical integrations required to obtain a good fit to the experimental energy distributions, the total ion yield, and the total neutral yield. We will not analyze the other ion energy distributions. The principal purpose of this analysis is to provide an additional and more quantitiative test of the plausibility of the model which has been proposed.

A schematic of the potential-energy diagram for adsorption is given in Fig. 11. M refers to a metal, and A refers to an adsorbed particle. For simplicity, we consider only the ground state $(M+A)$ and the ionic state (M^-+A^+). The potential energy of the ground state and the ionic state are expressed by $V_G(X)$ and $V(X)$ as a function of distance X, respectively. The zero of the potential energy is taken as the ion A^+ at infinite distance from the surface. V_i is the ionization potential of the particle A in the gas phase, ϕ is the work function of the gas-covered metal, E_d is the activation energy for desorption of the particle A, and V_{TO} is the threshold energy to produce an A^+ ion of zero kinetic energy.

An electron incident on such a system can cause transitions from the ground state to the ionic state. Since the mass of the atom is much larger than that of the electron, these transitions are "vertical," that is, the position and the kinetic energy of the atom are constant during the transition (transition 1, Fig. 11).[32] Once excited, the ion is subjected to a strong repulsive force and moves away from the surface. The transitions such that the kinetic energy E_k of the ion after escape is greater than zero occur within the region on the X axis where the value of the potential energy of the M^-+A^+ curve is greater than the value at infinite distance from the surface, and where the wave function of the particle A in the ground state has a finite value.

If all of the ions produced in the excitations to the ionic state escape from the surface, the ion energy distribution $f_0(V)$ is determined by the reflection[33] of the probability density distribution of the particle A in the ground state through the potential-energy curve of the ionic state, i.e.,

$$f_0[V(X_i)] = -N\sigma_{ex}|\varphi_G(X_i)|^2 (dV/dX)^{-1}_{X=X_i} . \quad (1)$$

where N is the number of particles adsorbed in the ground state per unit area, σ_{ex} is the cross section for excitation of the particle A from the ground state to the ionic state, and $\varphi_G(X)$ is the wave function of the particle A in the ground state.

Some of the ions will be neutralized to the ground state near the surface by Auger processes. Depending on the amount of kinetic energy the ion gains before neutralization occurs, the particle will either be recaptured by the surface or escape as a neutral. The high probability of this neutralization process explains the very small value of the ion desorption cross sections observed in most systems. If the rate of neutralization is $R(X)$, the probability that an ion of velocity v moving through dX at X will be neutralized is

$$R(X)\left(\frac{dX}{v}\right) . \quad (2)$$

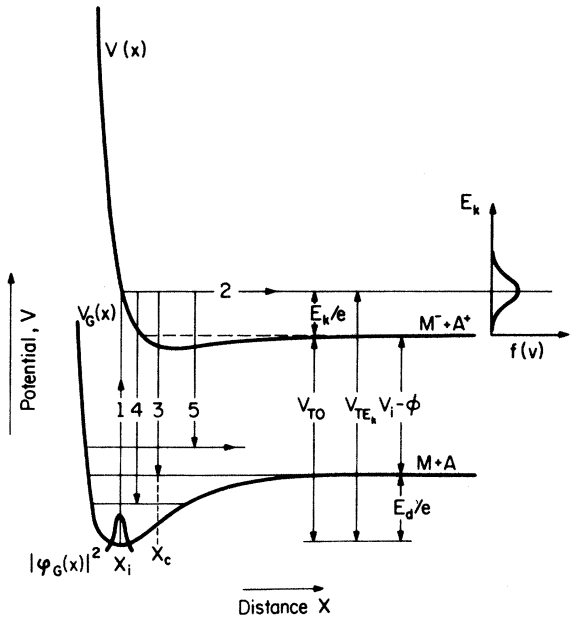

FIG. 11. Schematic of a simple potential-energy diagram for adsorption, showing the machanism of electron-impact desoption of the neutrals and ions.

If the particle A is excited into the ionic state at $X=X_i$, then the velocity v at the distance X is,

$$v=\{2q[V(X_i)-V(X)]/M\}^{1/2}, \tag{3}$$

where q is the ionic charge and M is the mass of the particle A.

Using Eq. (2), the probability $P(X_i)$ that an ion starts from $X-X_i$ and moves to infinity without being neutralized is

$$P(X_i)=\exp\left(-\int_{X_i}^{\infty} dX\frac{R(X)}{v}\right) . \tag{4}$$

Multiplying $P(X_i)$ [Eq. (4)] with $f_0\,[V(X_i)]$ [Eq. (1)], we get the energy distribution $f(V)$ of the desorbed ions

$$f[V(X_i)]=-N\sigma_{ex}|\varphi_G(X_i)|^2\frac{P(X_i)}{(dV/dX)_{X=X_i}} . \tag{5}$$

The total number N_T^+ of ions desorbed is

$$N_T^+=\int_0^{\infty} dV f[V(X_i)] . \tag{6}$$

An ion originating at X_i and moving away from the surface has kinetic energy $E_k=q[V(X_i)-V(X)]$ at the distance X. If neutralization occurs at $X\geq X_c$, where X_c is determined by

$$V(X_i)-V(X_c)=V_G(\infty)-V_G(X_c) , \tag{7}$$

the particle will have gained sufficient kinetic energy to surmount the potential barrier $[V_G(\infty)-V_G(X_c)]$ in the ground state, and desorption as a neutral will occur (transition 5, Fig. 11). X_c is of course a function of X_i. The total probability of desorption $P_T(X_i)$ (either as an ion or a neutral) for a particle excited at X_i is

$$P_T(X_i)=\exp\left(-\int_{X_i}^{X_c(X_i)} dX\frac{R(X)}{v}\right). \tag{8}$$

Multiplying $P_T(X_i)$ by the probability density distribution of the particle in the ground state $|\varphi_G(X_i)|^2$ and integrating over X_i, the total number of ions and neutrals desorbed per incident electron N_T can be calculated as

$$N_T=N\sigma_{ex}\int_{-\infty}^{+\infty} dX_i|\varphi_G(X_i)|^2P_T(X_i) . \tag{9}$$

We shall approximate the ground-state potential curve $V_G(X)$ by a Morse potential,[34]

$$V_G(X)=V_0(e^{-(2/d)X}-2e^{-(1/d)X}) . \tag{10}$$

where eV_0 is the activation energy for desorption (E_d) and d is the "width" parameter of the potential well. The wave function $\varphi_G(X)$ and the vibrational energy E_v of the particle in the ground state can be closely approximated by the solution for a harmonic oscillator,[35]

$$\varphi_G(X)=(\alpha/\pi^{1/2})^{1/2}\,e^{-(1/2)\alpha^2X^2}, \tag{11}$$

$$E_v=\hbar\omega_c , \tag{12}$$

where

$$\alpha=(M\omega_c/\hbar)^{1/2} , \tag{13}$$

and M is the mass of the particle. ω_c is given by

$$\omega_c=(1/d)\,(2V_0/M)^{1/2} . \tag{14}$$

The potential energy of an ion, $V(X)$, is approximated by

$$V(X)=Be^{-bX} , \tag{15}$$

the Born-Mayer repulsive potential resulting from the inner-core interaction.[36] The image potential and van der Waals and exchange forces are neglected. The reasons for neglecting these will be mentioned later.

We shall assume that the ions are neutralized near the surface by an Auger process and that the rate of neutralization $R(X)$ is given by[37]

$$R(X)=Ae^{-aX} . \tag{16}$$

Thus substituting Eqs. (15) and (16) into Eq. (4), the probability $P(X_i)$ that an ion starting from $X=X_i$ will move to infinity without being neutralized is

$$P(X_i)=\exp[-(A/b)\,(M/2qB)^{1/2}\times e^{-(a-b/2)X_i}F(p,\infty)] , \tag{17}$$

where q is the ionic charge,

$$p = a/b \ , \tag{18}$$

$$F(p,u) = \int_0^u du[e^{-pu}/(1-e^{-u})^{1/2}], \tag{19}$$

$$F(p,\infty) = (\sqrt{\pi})[\Gamma(p)/\Gamma(p+\tfrac{1}{2})] \ , \tag{20}$$

and

$$\Gamma(p) = \int_0^\infty du u^{p-1} e^{-u} . \tag{21}$$

Therefore, using Eq. (5), the energy distribution of ions is

$$f[V(X_i)] = -\frac{\alpha N\sigma_{ex}}{\pi^{1/2}} \exp\left[-\alpha^2 X_i^2 - \frac{A}{b}\left(\frac{M}{2qB}\right)^{1/2} \times e^{-(a-b/2)X_i} F(p,\infty)\right] \left|\frac{dX}{dV}\right|_{X=X_i} . \tag{22}$$

Expressing X_i in terms of V [Eq. (15)], the distribution $f(V)$ is given by

$$f(V) = \frac{\alpha N\sigma_{ex}}{b\pi^{1/2}V} \exp\left[-\alpha^2\left(\frac{1}{b}\ln\frac{V}{B}\right)^2 - \frac{A}{b}\left(\frac{M}{2qB}\right)^{1/2}\left(\frac{V}{B}\right)^{p-1/2} F(p,\infty)\right] . \tag{23}$$

Using Eq. (6), the total ion yield N_T^+ is given by

$$N_T^+ = \frac{\alpha N\sigma_{ex}}{b\pi^{1/2}} \int_0^\infty \frac{dV}{V} \exp\left[-\alpha^2\left(\frac{1}{b}\ln\frac{V}{B}\right)^2 - \frac{A}{b}\left(\frac{M}{2qB}\right)^{1/2}\left(\frac{V}{B}\right)^{p-1/2} F(p,\infty)\right] . \tag{24}$$

We have defined a critical distance X_c by Eq. (7). In terms of the potentials which we have assumed, X_c is given by

$$B(e^{-bX_i} - e^{-bX_c}) = V_0(2e^{-(1/d)X_c} - e^{-(2/d)X_c}) \ . \tag{25}$$

Using Eq. (8), the probability $P_T(X_i)$ that an ion starting at $X = X_i$ will move to $X = X_c(X_i)$ without being neutralized is

$$P_T(X_i) = \exp\left\{-\frac{A}{b}\left(\frac{M}{2qB}\right)^{1/2} e^{-(a-b/2)X_i} \times F[p, b(X_c(X_i) - X_i)]\right\} . \tag{26}$$

Using Eq. (9), the total number of ions and neurals desorbed per incident electron N_T is

$$N_T = N\sigma_{ex}\alpha(\pi)^{-1/2}\int_{-\infty}^{\infty} dX_i \exp\left[-\alpha^2 X_i^2 - \frac{A}{b}\left(\frac{M}{2qB}\right)^{1/2} \times e^{-(a-b/2)X_i} F[p, b(X_c(X_i) - X_i)]\right] . \tag{27}$$

Using Eqs. (24) and (27), the ratio R of the number of neutrals to the number of ions desorbed per incident electron is

$$R = (N_T - N_T^+)/N_T^+ . \tag{28}$$

We have used Eqs. (23), (24), and (27) to calculate the energy distribution of ions $f(V)$, the total ion yield N_T^+, and the total number of ions and neutrals desorbed per incident electron N_T, for O^+ from O_2/W and CO/W. An iterative process (described below) is used to determine the values of the parameters a, A, b, and B which produce a fit to the experimental results. Integrals are calculated numerically by the use of a computer.

1. O^+ *Ions from the* O_2/W *System*

The activation energy V_0 for desorption of an oxygen atom from the ground state is taken as 6.5 eV. The vibrational energy E_V of an oxygen atom adsorbed on tungsten is estimated to be 75 meV.[38] Using Eqs. (12)–(14), these assumptions give $\alpha = 17$ Å^{-1} and $d = 0.77$ Å. Assuming an initial excitation cross section σ_{ex} which is ~10 times the value of the ionization cross section of an oxygen atom in the gas phase,[39] and a surface coverage N of $\sim 3\times10^{13}$ atoms/cm^2, the number of O^+ ions excited into the ionic state by a single electron ($N\sigma_{ex}$) is estimated to be ~0.1. The values reported for the number of O^+ ions desorbed per incident electron vary among researchers (Table I). On the basis of the approximations indicated previously, we have estimated in this work that the yield is 10^{-5} ions/electron. However, the retarding-field analyzer is best suited for the measurement of ion yields, and we shall use a value of 1.0×10^{-6} O^+ ions per incident electron as reported by Madey and Yates.[26] We also assume that 1.0×10^{-4} O^+ ions. and neutrals are liberated per incident electron. This number is estimated on the basis of our measurement of the total desorption cross section (3×10^{-18} cm^2) and an assumed surface coverage of 3×10^{13} atoms/cm^2. This means that if one atom is excited into the ionic state, it has a probability of 1.0×10^{-5} of leaving as an ion and a probability of 1.0×10^{-3} of leaving as a neutral.

As the first step in the calculation, we obtain a rough estimate of the values of the parameters a, A, b, and B required to give the observed values for the number of ions and neutrals desorbed. Since the probability density distribution $|\varphi_G(X)|^2$ of the oxygen atom in the ground state is strongly peaked at $X = 0$, we make the approximation that an oxygen atom is excited only at this position, i.e., $X_i = 0$. Then, using Eq. (17),

$$\exp\left[-\frac{A}{b}\left(\frac{M}{2qB}\right)^{1/2}(\sqrt{\pi})\frac{\Gamma(p)}{\Gamma(p+\frac{1}{2})}\right] \approx 1\times10^{-5} . \tag{29}$$

Using Eq. (25),

$$B(1-e^{-bX_c}) \approx V_0(2e^{-(1/d)X_c} - e^{-(2/d)X_c}) . \quad (30)$$

Using Eq. (26),

$$\exp[-(A/b)(M/2qB)^{1/2} F(p, bX_c)] \approx 1\times10^{-3} . \quad (31)$$

Since 8.8-eV O^+ ions (the peak in the energy distribution) are initially excited at $X \approx 0$ (Fig. 11), we take $B = 8.8$ eV. Using Eqs. (29), (30), and (31), the values of a, A, and X_c are determined for various values of b. The results calculated with the aid of a computer are shown in Fig. 12. From these curves, we can determine values for a and A after selecting a reasonable value for b. For example, as a trial, we can choose $b = 3.5$ Å^{-1}, which gives $a = 1.8$ Å^{-1} and $A = 1.4\times10^{15}$ sec^{-1}. Putting these values into Eqs. (24) and (27), we can calculate N_T^+ and N_T. Doing this, we find $N_T^+ = 6.0\times10^{-7}$ (ions/electron) and $N_T = 6.6\times10^{-5}$ (ions and neutrals/electron). As we have determined the values of a, A, b, and B considering ions which are excited only at $X = X_i = 0$, it is quite natural that the calculated values of N_T^+ and N_T are different from those which we have initially assumed. Trying a few more values of b and the corresponding values of a and A, we get a set of values for these parameters that gives the calculated values for N_T^+ and N_T, which are reasonably close to the values that we have assumed originally. Thus, for $b = 3.8$ Å^{-1}, $a = 1.9$ Å^{-1}, and $A = 1.4\times10^{15}$ sec^{-1}, we get $N_T^+ = 1.2\times10^{-6}$ (ions/electron) and $N_T = 1.1\times10^{-4}$ (ions and neutrals/electron).

As the second step, we put these values of a, A, b, and B into Eq. (23) and calculate the energy distribution of O^+ ions. For $B = 8.8$ eV, the calculated energy distribution has a peak at 8.5 eV, but the shape of the distribution is fairly close to the one which has been measured. In order to shift the energy peak to 8.8 eV, the value of B is changed,

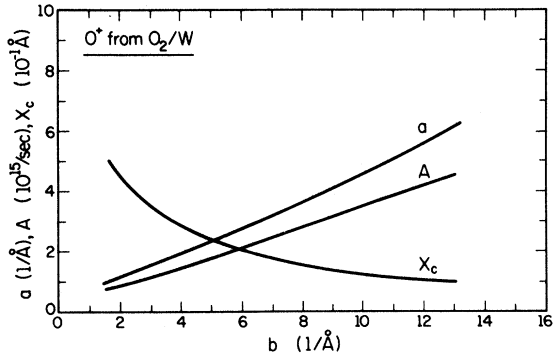

FIG. 12. Relation of the parameters a, A, X_c, and b for the theoretical calculation of the energy distribution of O^+ ions from O_2/W ($B = 8.8$ eV).

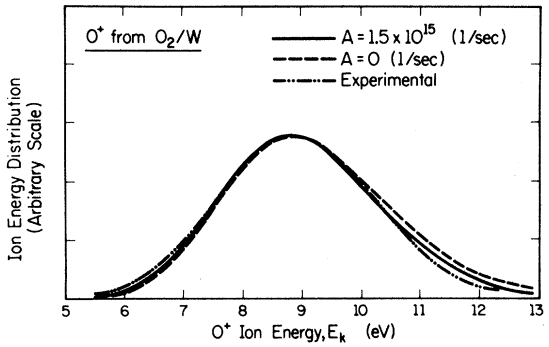

FIG. 13. Comparison of the calculated energy distribution of O^+ ions from O_2/W with the experimental result (Fig. 2). The calculated energy distribution of O^+ ions without taking the neutralization process into consideration is shown also. The curve neglecting neutralization is multiplied by 10^{-5} to normalize it at the maxima of the other curves.

with the values of the rest of the parameters remaining the same. In this case, $B = 9.1$ eV puts the maximum of the calculated distribution at 8.8 eV. When the value of B is changed, the calculated values of N_T^+ and N_T also change. For $B = 9.1$ eV, we find $N_T^+ = 1.5\times10^{-6}$ (ions/electron) and $N_T = 1.4\times10^{-4}$ (ions and neutrals/electron).

The set of values for the parameters which we have obtained at this point gives fairly good values for N_T^+ and N_T, and yields a good approximation to the observed energy distribution of O^+ ions. The next step is to set $B = 9.1$ eV and go back to the first step, calculating new values of the parameters a, A, and b. This is the starting point of the iterative process. We proceed through the whole cycle until reasonable values result. The values of the parameters which give a good fit are $a = 2.0$ Å^{-1}, $A = 1.5\times10^{15}$ sec^{-1}, $b = 3.7$ Å^{-1}, and $B = 9.1$ eV. These values give a total O^+ ion yield N_T^+, of 9.4×10^{-7} (ions/electron), the total number of O^+ ions and neutrals desorbed per incident electron N_T of 7.9×10^{-5} (ions and neutrals/electron), and a ratio R of the number of the desorbed neutrals to ions of 84.

Figure 13 shows a comparison of the calculated energy distribution of O^+ ions with the experimental distribution. The calculated energy distribution of O^+ ions without taking the neutralization process into consideration is shown also. The curve neglecting neutralization is mulitplied by 10^{-5} to normalize it as the maxima of the other curves. Figure 14 shows plots of the ground-state potential energy $V_G(X)$, the probability density distribution $|\varphi_G(X)|^2$, the ionic-state potential energy $V(X)$, and the calculated energy distribution.

In our treatment, we have neglected the contri-

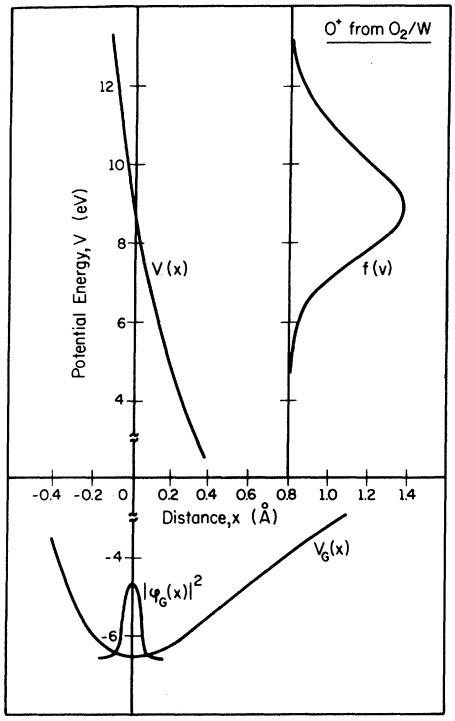

FIG. 14. Plots of the potential energy $V_G(X)$ of an oxygen atom in the ground state, the probability density distribution $|\varphi_G(X)|^2$, of an oxygen atom in the ground state, the potential energy $V(X)$ of an O^+ ion in the ionic state, and the calculated energy distribution $f(V)$ of O^+ ions (O_2/W).

bution of the image potential to the potential curve for ions. Since the width of the probability density distribution of the ground-state oxygen atom is only ~0.2 Å, the primary influence of the potential curve is through its slope, dV/dX. The slope of the Born-Mayer potential is ~34 V/Å at $X=0$, while the slope of the image potential is ~1 V/Å (assuming that the equilibrium spacing between tungsten and an O^+ ion is ~2 Å). Since the latter is quite small compared to the former, we are justified in neglecting the image potential. A similar argument applies to van der Waals and exchange forces.

2. O^+ *Ions from the* CO/W *System*

The activation energy V_0 for desorption of an oxygen atom in the ground state is taken as 5.2 eV. The vibrational energy E_V of α-CO adsorbed on tungsten is taken to be 258 meV.[38] This corresponds to $\alpha = 32\,(1/\text{Å})$ and $d = 0.20$ Å. We assume that the number of O^+ ions excited into the ionic state by a single electron $N\sigma_{ex}$ is ~0.1. The values for the number of O^+ ions desorbed per incident electron vary among researchers (Table I). We assume that 4×10^{-6} O^+ ions are desorbed per incident electron. We also assume that 5×10^{-4} O^+ ions and neutrals are liberated per incident electron. The ratio of the desorbed neutrals to ions is then about 125.

Following an iterative process similar to the one described for the case of O^+ ions from the O_2/W system, we obtain values of parameters which predict the experimental results well. The values are $a = 3.3$ Å^{-1}, $A = 2.1\times10^{15}$ sec^{-1}, $b = 6.6$ Å^{-1}, and $B = 8.1$ eV. The values of N_T^+ and N_T calculated from these parameters are 3.8×10^{-6} (ions/electron) and 5.0×10^{-4} (ions and neutrals/electron). The ratio of the desorbed neutrals to ions is 132.

Figure 15 shows a comparison of the calculated energy distribution of O^+ ions with the experimental result. The calculated energy distribution of O^+ ions without taking the neutralization process into consideration is also shown. The curve neglecting neutralization is multiplied by 4×10^{-5} to normalize it at the maxima of the other curves.

It is interesting to note that, since in both of these cases the shape of the curves calculated with and without neutralization are essentially the same, the probability of escape of an ion is almost independent of the position of excitation. This is a result of the very strong localization of the nucleus in the ground state. Having demonstrated this fact for fairly reasonable values for the various parameters derived in this calculation, we could produce a much simpler approach to the calculation. In particular, we see that the shape of the distribution is determined only by the parameter α in the ground-state wave function and the slope of the ion interaction potential.

The relationship between the interaction potentials for the ion $V(X)$ and for the neutral $V_G(X)$

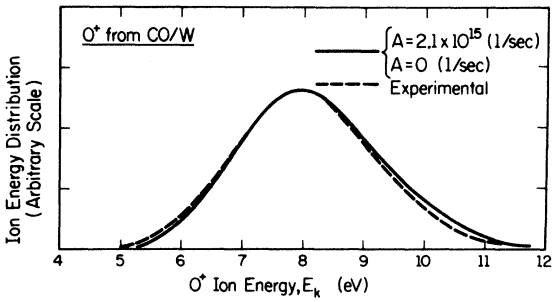

FIG. 15. Comparison of the calculated energy distribution of O^+ ions from CO/W with experimental result (Fig. 4). The calculated energy distribution without taking the neutralization process into consideration is shown also. The curve neglecting neutralization is multiplied by 4×10^{-5} to normalize it at the maxima of the other curves.

has a substantial effect on the energy distribution of the emitted ions. In the case of O^+ emission from all of the systems, $V(X)$ is greater than zero over the entire region where the wave function $\varphi_G(X)$ of the ground state is finite (Fig. 14). This assertion can be made since in every case the minimum kinetic energy of the emitted ions is greater than zero. In contrast to this situation, the energy distributions for H^+ ions from H_2/W and H_2O/W appear to start at zero kinetic energy. This shows that for these systems $V(X)$ passes through zero in the region where $\varphi(X)$ is finite. Such a relationship would also produce asymmetrical distributions as observed for these cases. It would appear that the analysis outlined above would apply to these systems also. An exception would be that $V(X)$ could not be approximated by a simple Born-Mayer potential but would have to have an attractive component.

The calculations described above were made as an additional test of the qualitative validity of the model. As we do not have accurate values for N_T^+ and N_T, we have performed only a few cycles of the iterative process, that is, the values of N_T^+ and N_T calculated are not exactly the same as those estimated, but we have shown that we can find a set of values for the parameters which give reasonable results for N_T^+ and N_T, and the measured energy distribution of O^+ ions. In addition, the values of the parameters are reasonable. Finally, we note that the above treatment is a one-dimensional calculation, and that the initial excitation to other states, e.g., antibonding states, has been neglected.

B. Threshold Energies

Reference to Fig. 11 shows that the minimum amount of energy required to excite an atom from the ground state of adsorption to the ionic state with no kinetic energy is

$$eV_i - e\phi + E_d \quad , \tag{32}$$

where V_i is the ionization potential, ϕ is the work function of the metal, and E_d is the activation energy for desorption of the absorbate atom. This excitation leaves the atomic electron at the Fermi level. On the other hand, the maximum amount of energy which an incident electron can give up in an electronic excitation is

$$eV_e + e\phi \quad , \tag{33}$$

where eV_e is the kinetic energy of the electron. Thus the threshold energy for excitation to the zero-kinetic-energy ionic state is given by

$$eV_e + e\phi = eV_i - e\phi + E_d \quad , \tag{34}$$

and the threshold energy for excitation to an ionic state with kinetic energy E_k is

$$eV_e = eV_i + E_d + E_k - 2e\phi \quad . \tag{35}$$

Equation (35) will hold for the situation in which both the electron originally on the adsorbed atom and the incident electron go to the Fermi level. This is then the "absolute" threshold. If for some reason the probability of this occurring is either zero or extremely small, the threshold which is observed will be at a higher energy. Such a higher "observed" threshold could occur, for example, in the case where the adsorbate particle is at a substantial distance from the surface. Thus, the overlap integral between the atomic electronic state and the metallic electronic state for the Fermi level would be extremely small, and the probability for transitions at the absolute threshold would be correspondingly small. For such cases, the threshold would be somewhere between the energies given by Eq. (35) and

$$eV_e = eV_i + E_d + E_k \quad . \tag{36}$$

The transition represented by this latter expression leaves both of the electrons at the vacuum level.

We shall apply these expressions to the analysis of the thresholds which we have obtained in the present work. We have, in general, found threshold values smaller than those reported previously in the literature. This is possibly due to the higher sensitivity of our systems. As pointed out previously, in this apparatus this measurement is for a specific ion energy (whereas, in retarding-potential and mass-spectrometer systems the equivalent measurement is for a range of energies greater than some minimum value). Thus the gradual rise near threshold (e.g., Fig. 10) is not due to the mixing of ion energies but is the real behavior for a single-ion energy. It seems likely that this very gradual rise is a reflection of the fact that the electrons do in fact tend to end up in states below the vacuum level but with rapidly decreasing probability.

Table II summarizes the threshold measurements made in the present work along with those made by other workers. Theoretical threshold energies are given for two cases: (a) the final states of the two electrons are at the vacuum level, and (b) the final states of the two electrons are at the Fermi level. The assumptions made to calculate the theoretical threshold energies are

O_2/W:

(1) the work function of oxygen-covered tungsten, 5.9 eV;

(2) the activation energy for the desorption of an oxygen atom from oxygen-covered tungsten, 6.5 eV;

CO/W:

(1) the work function of CO-covered tungsten,

5.3 eV;

(2) the activation energy for desorption of state 1-CO from tungsten, 1.0 eV;

(3) the activation energy for the desorption of state 2-CO from tungsten, 1.1 eV;

(4) the activation energy for the desorption of a carbon atom from tungsten, 7 eV.

For O^+ from O_2/W and CO/W, it will be noted that our measurement is approximately 2.5–3 eV lower than any of the previous measurements and that our value is considerably closer to the value predicted by Eq. (35), that is, to the case where both electrons end up at the Fermi level. In contrast to this, the threshold for CO^+ ions from CO/W is quite close to the value predicted by the model where both electrons end up at the vacuum level. It seems plausible that the difference is due to the fact that the CO^+ ions come from a weakly bound state which is adsorbed over previously adsorbed CO and is thus at a larger distance from the surface.

Even though the threshold measurements are difficult to make because of the gradual rise in the ion current over a rather wide range of electron energy, we feel that we have shown that the threshold for tightly bound states is not given by either the model in which both electrons end up at the vacuum level as proposed by Redhead[2] nor by the model where one electron ends up at the vacuum level and the other at the Fermi level as proposed by Menzel and Gomer.[3] However, for the case where the adsorbate particle is at a relatively large distance from the surface, the "apparent" threshold may be given by assuming that both of the electrons end up at the vacuum level.

V. SUMMARY

We have designed and constructed a cylindrical magnetic spectrometer for the study of the electron-impact desorption of ions and neutrals from solid surfaces. The apparatus has been applied to the study of polycrystalline tungsten with O_2, CO, H_2, N_2, CO_2, and H_2O adsorbed. Some of the results are:

(1) The ions which have been observed are O^+ from O_2/W, CO/W, and CO_2/W; CO^+ from CO/W; and H^+ from H_2/W and H_2O/W.

(2) The analysis of the observed O^+ ion-energy distributions for the O_2/W and CO/W systems indicates the qualitative validity of the model for the mechanism of electron-impact desorption of ions and neutrals as proposed by Redhead, and Menzel and Gomer.

(3) The dependence of the O^+ ion desorption cross section and total desorption cross section for O_2/W on electron energy indicates that the neutralization of ions is not the only mechanism but is a dominant mechanism for neutral desorption.

(4) Typically, the ion desorption cross sections increase sharply with V_e for $V_e \lesssim 100$ eV and increase slowly for $V_e \gtrsim 100$ eV.

(5) The threshold energies measured are substantially lower than those previously reported. Theoretical threshold energies agree reasonably well with the experimental results.

---

*This work was supported in part by the Joint Services Electronics Programs (U. S. Army, U. S. Navy, and U. S. Air Force) under Contract No. DAAB-07-67-C-0199.

†Present address: Central Research Laboratory, Mitsubishi Electronic Co., 80 Nakano, Minami-shimizu, Amagasaki, Japan.

[1]A. J. Dempster, Phys. Rev. 11, 316 (1918).

[2]P. A. Redhead, Can. J. Phys. 42, 886 (1964).

[3]D. Menzel and R. Gomer, J. Chem. Phys. 41, 3311 (1964).

[4]W. C. Schuemann, J. L. deSegovia, and D. Alpert, Translation of the Tenth National Vacuum Symposium, 1963, p. 223 (unpublished).

[5]T. E. Hartman, Rev. Sci. Instr. 34, 1190 (1963).

[6]P. A. Readhead, Vacuum 13, 253 (1963).

[7]L. A. Pétermann, Nuovo Cimento Suppl. 1, 601 (1963).

[8]F. A. Baker and L. A. Pétermann, J. Vac. Sci. Technol. 3. 285 (1966).

[9]J. L. Robins, Can. J. Phys. 41, 1385 (1963).

[10]D. Lichtman, J. Vacuum Sci. Technol. 2, 70 (1965).

[11]D. Lichtman and T. R. Kirst, Phys. Letters 20, 7 (1966).

[12]D. Lichtman, T. R. Kirst, and R. B. McQuistan, Phys. Letters 20, 129 (1966).

[13]D. Lichtman, R. B. McQuistan, T. R. Kirst, Surface Sci. 5, 120 (1966).

[14]M. I. Datsiev and N. I. Ionov, Zh. Tekhn. Fiz. 37, 1140 (1967) [Soviet Phys. Tech. Phys. 12, 821 (1967)].

[15]D. R. Sandstrom, J. H. Leck, and E. E. Donaldson, J. Appl. Phys. 38, 2851 (1967).

[16]D. Lichtman, F. N. Simon, and T. R. Kirst, Surface Sci. 9, 325 (1968).

[17]F. N. Simon, D. Lichtman, and T. R. Kirst, Surface Sci. 12, 299 (1968).

[18]J. W. Coburn, Surface Sci. 11, 61 (1968).

[19]D. Menzel, Ber. Bunsenges. Physik. Chem. 72, 591 (1968).

[20]D. Menzel and R. Gomer, J. Chem. Phys. 40, 1164 (1964).

[21]D. Menzel and R. Gomer, J. Chem. Phys. 41, 3329 (1964).

[22]W. Ermich, Philips Res. Rept. 20, 94 (1965).

[23]P. A. Redhead, J. Appl. Phys. Letters 9, 166 (1964).

[24]P. A. Redhead, Nuovo Cimento Suppl. 5, 586 (1967).

[25]J. T. Yates, Jr., T. E. Madey, and J. K. Payn, Nuovo Cimento Suppl. 5, 558 (1967).

[26]T. Madey and J. T. Yates, Jr., Surface Sci. 11, 327 (1968).
[27]M. Nishijima and F. M. Propst, J. Vacuum Sci. Technol. 7, 420 (1970).
[28]M. Nishijima and F. M. Propst, J. Vacuum Sci. Technol. 7, 410 (1970).
[29]J. A. Becker, E. J. Becker, and R. G. Brandes, J. Appl. Phys. 32, 411 (1961).
[30]V. S. Fomenko, in *Handbook of Thermionic Properties*, edited by G. V. Samsonov,
[31]R. V. Culver and F. C. Tompkins, in *Advances in Catalysis*, edited by D. D. Eley, P. W. Selwood, and P. B. Weisz (Academic, New York, 1959), Vol. 11, p. 97.
[32]J. Franck, Trans. Faraday Soc. 21, 536 (1926); E. U. Condon, Phys. Rev. 28, 1182 (1926); 32, 858 (1928).
[33]H. D. Hagstrum, Rev. Mod. Phys. 23, 185 (1951).
[34]P. M. Morse, Phys. Rev. 34, 57 (1929).
[35]L. Pauling and E. B. Wilson, Jr., *Introduction to Quantum Mechanics with Application to Chemistry* (McGraw-Hill, New York, 1935).
[36]M. Born and J. E. Mayer, Z. Physik 75, 1 (1932).
[37]H. D. Hagstrum, Phys. Rev. 96, 336 (1954).
[38]F. M. Propst and T. C. Piper, J. Vacuum Sci. Technol. 4, 53 (1967).
[39]F. M. Propst and E. Lüscher, Phys. Rev. 132, 1037 (1963).

PHYSICAL REVIEW B VOLUME 2, NUMBER 7 1 OCTOBER 1970

Mössbauer Spectroscopy in Group-III Antimonides*

R. A. Pruitt† and S. W. Marshall
Department of Physics, Colorado State University, Fort Collins, Colorado 80521
and
C. M. O'Donnell
Department of Chemistry, Colorado State University, Fort Collins, Colorado 80521
(Received 16 April 1970)

Mössbauer absorption spectra of the group-III antimonides AlSb, GaSb, and InSb, and ternary alloys of the latter two compounds have been taken at 78 °K, using the 37.2-keV, $\frac{7}{2}^+ \rightarrow \frac{5}{2}^+$ transition in Sb^{121}. An absorber of $KSbF_6$ was used to help determine the nuclear factor $\delta R/R = (-6.7 \pm 3) \times 10^{-4}$. Chemical bonding in these compounds has both ionic and covalent character raising the question of relative ionicity. Molecular-orbital (MO) and linear-combination-of-atomic-orbital calculations, together with an assessment of electronegativity differences, predict that ionicity increases for the series GaSb, InSb, and AlSb, whereas measurements of the Mössbauer isomer shift along with some bulk and atomic properties show that ionicity increases in the series InSb, GaSb, and AlSb. Interpretation of the isomer-shift data is somewhat complicated by shielding of the p electrons at the Sb nucleus, but electron populations determined by MO calculations indicate that the $5s$-electron population is nearly the same on the Sb nuclei in the three compounds, in accord with the results of Hafemeister *et al.* on alkali iodides and those of Lees and Flinn on tin compounds. Thus, the $5s$-electron population tends to be constant in compounds of these three elements from the same row of the periodic chart. Though the single-line Mössbauer absorption spectra were broad for some absorbers, there was no evidence of quadrupole hyperfine structure which would have been apparent from asymmetry of the absorption lines.

I. INTRODUCTION

In the absence of hyperfine splitting, Mössbauer absorption lines unambiguously reflect the relative electron densities, measured at the nucleus, between absorbers composed of different solid materials. Since the isomer-shift δ may be written as the product of an electronic factor and a nuclear factor, the electron densities may be *measured* only after the nuclear factor for a particular γ-ray transition has been determined. In this paper we discuss results obtained from Mössbauer experiments using γ rays from the 37.2-keV, $\frac{7}{2}^+ \rightarrow \frac{5}{2}$ transition in[1] Sb^{121} which, together with calculations of electron densities arising from various configurations, have permitted determination of the nuclear factor for this transition. We have used the nuclear-factor and isomer-shift measurements on the group-III antimonides, AlSb, GaSb, and InSb, to measure the degree of ionicity in these compounds, in a manner similar to that of Hafemeister *et al.* for compounds of iodine.[2] The ternary alloys $Ga_xIn_{1-x}Sb$ were studied as well to see